Trajectory evolution in the multi-body problem with applications in the Saturnian System

ARTICLE *in* ACTA ASTRONAUTICA · SEPTEMBER 2011

Impact Factor: 0.82 · DOI: 10.1016/j.actaastro.2011.07.007

Acta Astronautica 69 (2011) 1038–1049

Contents lists available at ScienceDirect

Acta Astronautica

journal homepage: www.elsevier.com/locate/actaastro

Trajectory evolution in the multi-body problem with applications in the Saturnian system ☆

Diane Craig Davis, Kathleen C. Howell *

School of Aeronautics and Astronautics, Purdue University, West Lafayette, IN, USA

ARTICLE INFO

Article history:
Received 1 February 2011
Received in revised form
1 July 2011
Accepted 11 July 2011
Available online 15 August 2011

Keywords:
Trajectory design
Multi-body dynamics
Three-body problem
Periapsis Poincaré maps

ABSTRACT

Recent discoveries by the Cassini spacecraft have generated interest in future missions to further explore the moons of Saturn as well as other small bodies in the solar system. Incorporating multi-body dynamics into the preliminary design can aid the design process and potentially reduce the cost of maneuvers that are required to achieve certain objectives. The focus in this investigation is the development and application of additional design tools to facilitate preliminary trajectory design in a multi-body environment where the gravitational influence of both primaries is quite significant. Within the context of the circular restricted 3-body problem, then, the evolution of trajectories in the vicinity of the smaller primary (P_2) that are strongly influenced by the distant larger primary (P_1) is investigated. By parameterizing the orbits in terms of radius and periapse orientation relative to the P_1–P_2 line, the short- and long-term behaviors of the trajectories are predictable. Initial conditions that yield a trajectory with a particular set of desired characteristics are easily selected from periapsis Poincaré maps for both short- and long-term orbits. Analysis in the Sun–Saturn and Saturn–Titan systems serves as the basis for examples of mission design applications.

1. Introduction

Increasingly complex spacecraft mission scenarios demand innovative trajectory design concepts and the development of computational tools that incorporate the dynamical structure of the design space. In support of wide-ranging exploration goals, any one vehicle may fly through various types of dynamical regimes during a single mission. Exploiting the dynamical structure in different force environments may offer advantages in trajectory design. In regimes where multiple bodies impact the spacecraft behavior to a similar degree, multiple gravity fields must be simultaneously considered even for preliminary design. However, multi-body environments are not as well understood as those involving a single gravitational body, and preliminary design in these complicated scenarios is challenging.

A major barrier to the development of a simple orbit design process is the overwhelming nature of the design space. With the addition of only one gravitational body, an analytical solution to the orbit problem is no longer available, and for large orbits, the ordered world of conic sections becomes an apparently chaotic regime, where predicting the long-term behavior of a trajectory based on its initial state is not straightforward. Even in the Circular Restricted 3-Body Problem (CR3BP), orbit design remains challenging due to the chaotic and varied nature of trajectories that are simultaneously influenced by two gravitational bodies. To effectively select a trajectory to satisfy a given design requirement, it is necessary to simplify and organize the design space. Concentrating on the region in the vicinity of the smaller primary, this effort focuses on the development of strategies that

☆ This paper was presented during the 61st IAC in Prague.

* Corresponding author.
E-mail addresses: decraig@purdue.edu (D.C. Davis), howell@purdue.edu (K.C. Howell).

0094-5765/$ - see front matter © 2011 Elsevier Ltd. All rights reserved.
doi:10.1016/j.actaastro.2011.07.007

facilitate preliminary trajectory design in the CR3BP. Rather than attempting to cancel out the multi-body gravitational perturbations, these schemes exploit the additional gravitational forces to facilitate the design of trajectories and potentially expose options that may otherwise not be apparent.

Numerous investigators now exploit tidal acceleration in mission applications. For example, Belbruno [1] develops the concept of ballistic lunar transfers, which enlist the Sun's gravity to pull a spacecraft from the vicinity of the Earth out to the vicinity of the Moon. This type of transfer, one that requires significantly less ΔV than a traditional Hohmann transfer, was employed by the Japanese spacecraft Hiten to reach the Moon in 1991, as described by Belbruno and Miller [2]. Yamakawa et al. [3] present an approach for the design of such trajectories, investigating the tidal acceleration of P_1 on an orbiter at P_2. In a further study by Kawaguchi et al. [4], the methods are applied to the design of trajectories for the LUNAR-A mission to the Moon and the PLANET-B mission to Mars.

In an attempt to better understand the dynamics involved in the three-body problem and to facilitate trajectory design, manifolds associated with periodic orbits in the CR3BP have been increasingly used to predict the long-term behavior of trajectories that originate near the smaller primary. Many examples of this type of analysis exist in the literature. Howell and Kakoi [5] compute free connections between Earth–Moon libration point orbits and Sun–Earth libration point orbits by connecting the manifolds of the two types of orbits. Koon et al. [6], as well as Gómez et al. [7] connect stable and unstable manifolds in the various Jupiter–moon systems to produce a "Petit Grand Tour" of the moons, which includes flybys of Europa and Ganymede that require low ΔV. Parker and Born [8] approach the ballistic lunar transfer problem in terms of manifolds in the Sun–Earth and Earth–Moon systems. Russell and Lam [9] select several large, unstable orbits about P_2, and using the associated stable manifolds, design transfer trajectories into each periodic orbit. Applying multi-body dynamics to examine the behavior of natural bodies, Howell et al. [10] describe the behavior of comets Oterma and Helin-Roman-Crocket in terms of stable and unstable halo manifolds in the Sun–Jupiter system.

One major challenge involved in orbit design within the context of the CR3BP is the organization of the vast set of options that is available within the design space; it is challenging to locate the specific initial conditions that lead to a trajectory with particular characteristics. One method for visualizing the space is the use of Poincaré maps, which reduce the dimensionality of the problem. Commonly, maps are projected onto a physical plane. In the CR3BP, such a projection is often realized on the plane defined by $y=0$, and the returns to the map are plotted for trajectories with a particular Jacobi constant. Such maps are successfully employed in analyses such as Howell and Kakoi [5], Koon et al. [6], Gómez et al. [7], and Howell et al. [10]. A slightly different approach is to define the surface of section at the plane corresponding to periapsis. This type of map is known as a periapsis Poincaré map and is employed by Villac and Scheeres [11] to relate a trajectory escaping the vicinity of P_2 back to its previous periapsis in the planar Hill problem. The maps produce lobes corresponding to immediate escape; any trajectory at a given value of Jacobi constant that achieves periapsis within the corresponding lobe escapes before reaching a subsequent periapsis. The authors apply this observation to the design of escape trajectories from a circular orbit about Europa and other planetary satellites. Paskowitz and Scheeres [12] extend this analysis, using periapsis Poincaré maps to define lobes corresponding to the first four periapse passages after capture into orbit about P_2. Villac and Scheeres [13] also use periapsis Poincaré maps in the design of optimal plane change maneuvers, utilizing third-body forces to change the inclination of a trajectory with minimal ΔV. The periapsis Poincaré maps represent a very useful parameterization for the characterization of the design space in the vicinity of P_2.

This analysis was motivated in part by an earlier study of the design options for a set of wide-ranging end-of-mission scenarios for the Cassini spacecraft. Exploiting the natural dynamics in the multi-body environment to the greatest extent, and blending such arcs with those designed in other dynamical regimes, would have been greatly facilitated by a better understanding and organization of the multi-body design space. A process to select initial conditions along any arc that deliver a set of desired characteristics would have greatly increased the efficiency of the exploration process. Thus, this current investigation considers both short-term and long-term behavior of trajectories evolving in the vicinity of P_2 in the CR3BP. Periapsis Poincaré maps are employed to define sets of initial conditions for which trajectories impact or escape the vicinity of P_2 through the L_1 and L_2 gateways, to identify regions of initial conditions resulting in specific trajectory behavior over long term propagations, to locate quasi-periodic trajectories in both the rotating and inertial frames of reference, and to identify trajectories with other notable characteristics. These orbit selection techniques are applied to mission design examples in the Sun–Saturn and Saturn–Titan systems to demonstrate their application. Within a regime where trajectory behavior is heavily influenced by tidal acceleration, these periapsis Poincaré maps can expand a set of trajectory planning tools and enable a more methodical use of multiple gravity fields to design trajectories, some of which may otherwise not emerge as candidate solutions.

2. Background

2.1. Dynamical model

The motion of a spacecraft under the gravitational influence of two larger bodies, such as the Sun and a planet, can be described in terms of the CR3BP [14]. The libration points L_1 and L_2 are depicted for the Sun–Saturn system in Fig. 1. Note that the magnitude of the Hill radius [15] is equal to

$$r_H = \left(\frac{\mu}{3}\right)^{1/3} \quad (1)$$

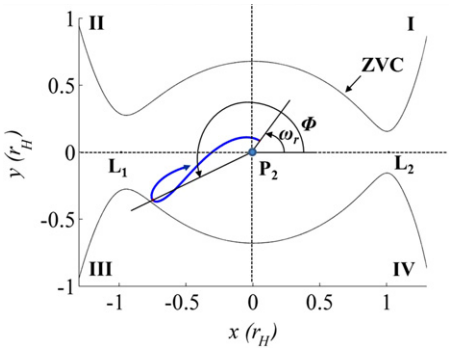

Fig. 1. P_2-centered trajectory with periapse angle ω_r and quadrant angle Φ.

and is approximately equal to the distance between P_2 and the libration points L_1 and L_2. A single integral of motion exists in the CR3BP. Known as the Jacobi integral, it is evaluated as

$$J = x^2 + y^2 + \frac{2\mu}{r} + \frac{2(1-\mu)}{d} - v^2 \tag{2}$$

where v is the magnitude of the spacecraft velocity relative to the rotating frame and d and r are the distances between the spacecraft and the first and second primaries, respectively. The Jacobi constant restricts the motion of the spacecraft to regions in space where $v^2 \geq 0$; these regions are bounded by surfaces of zero velocity. In the planar problem, the surfaces reduce to the zero velocity curves (ZVCs). When the value of the Jacobi integral decreases below the value associated with L_2, the ZVCs open at L_2 (see Fig. 1) and the spacecraft may escape entirely from the vicinity of the primaries.

2.2. Out-of-plane behavior

In the planar case, for each (x, y) position coordinate of a given periapsis point, the velocity magnitude is specified by the Jacobi constant, and the velocity direction is specified by the apse condition, which requires the velocity to be perpendicular to the position vector. Hence the position coordinate defines a single prograde trajectory. In 3D space, however, the velocity direction is no longer completely constrained by the (x, y, z) position coordinate; the apse condition only restricts the velocity to a plane normal to the position vector. To manage this complication, a plane is defined at r_{p0} such that the position vector is normal to the plane. Then, a velocity angle is introduced in this plane to isolate the velocity direction. Consider a trajectory characterized by a periapsis located at a particular position in space denoted by (x, y, z). The velocity angle ϕ is defined as the angle between the x–y plane and the velocity vector, as depicted in Fig. 2.

2.3. Tidal acceleration by quadrants

The direction of the perturbing acceleration due to the gravity of P_1 on a spacecraft in an orbit about P_2 depends on the orientation of the spacecraft orbit relative to the two bodies. To facilitate the investigation of the gravitational

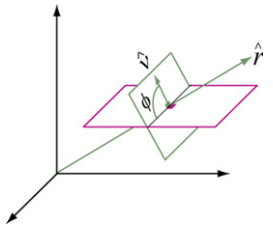

Fig. 2. Velocity angle ϕ between the x–y plane and the velocity vector.

influence of P_1, four quadrants centered at P_2 are defined in the rotating frame and are shown in Fig. 1. The quadrants are defined in a counterclockwise fashion, with quadrant I on the far side of the primary (relative to P_1) and leading P_2 in its orbit. When the spacecraft orbit is viewed in this rotating frame, its orientation is defined by the quadrant that contains the apoapsis on a given revolution. The quadrant angle Φ is the angle between the positive x-axis and apoapsis, as depicted in Fig. 1.

In the vicinity of P_2, the tidal acceleration is generally directed outwards from P_2 along the x-axis. The effects of the tidal acceleration on a P_2-centered orbit are greatest near apoapsis. In quadrants I and III, the perturbations generally oppose the direction of motion in a prograde orbit. In quadrants II and IV, on the other hand, the net perturbing acceleration at apoapsis is in the same direction as the motion along a prograde orbit. By comparing the osculating orbital elements measured at two subsequent periapses, these effects are quantized. Consider a prograde orbit sufficiently large to be impacted significantly by the gravity of P_2 but affected such that the perturbations do not cause the orbit to become retrograde or to escape the vicinity of P_2. If apoapsis lies in quadrant I or III, tidal acceleration lowers periapse radius, decreases semi-major axis, and increases eccentricity. Conversely, if apoapsis instead lies in quadrant II or IV tidal acceleration raises periapse radius, increases semi-major axis, and decreases eccentricity. For further discussion of changes in orbital elements due to tidal acceleration, see Yamakawa et al. [3], Villac et al. [16], and Davis et al. [17]. The gravitational perturbations due to P_1 are greatest when the orbit lies in the ecliptic plane. Also, within each quadrant, tidal perturbations are at a maximum when apoapsis lies at approximately 45° from the P_1–P_2 line, although the precise value is orbit-dependent.

2.4. Periapsis Poincaré maps

One tool that facilitates exploration of the design space near P_2 is the periapsis Poincaré map, first defined and introduced by Villac and Scheeres [11]. The Poincaré map is commonly used to interpret the behavior of groups of trajectories, relating the states at one point in time to a future state forward along the path. By fixing the value of the Jacobi integral and selecting a surface of section, the dimensionality of the problem is reduced by two; the four-dimensional planar problem is thus reduced to two dimensions. The surface of section can be a plane in configuration space, corresponding, for example, to $y=0$. However, another useful type of map is a periapsis Poincaré map [11,12]. In this type of map, the surface of section is the

plane of periapse passage, defined by the conditions $\dot{r}=0$ and $\ddot{r}>0$. Villac and Scheeres [11], as well as Paskowitz and Scheeres [12], employ periapsis Poincaré maps to explore the short-term behavior of escaping trajectories and capture trajectories within the context of the HR3BP with applications to the Jupiter–Europa system. Building on these results, the short-term behavior of trajectories in the CR3BP is explored; subsequently, periapsis Poincaré maps are employed to extract information concerning the long-term evolution of large P_2-centered trajectories.

For a given Jacobi value, the second condition defining periapsis, $\ddot{r}>0$, outlines a contour in the vicinity of P_2. Within the contour (see Figs. 3 and 4), a state satisfying the first condition, $\dot{r}=0$, is a periapsis; outside the contour, it is an apoapsis. For each position within the contour, the velocity is defined such that the initial state is a periapsis along a P_2-centered prograde trajectory. Each orbit is then parameterized by its initial polar coordinates: periapse radius r_{p0} and the angle with respect to the rotating x-axis, defined as ω_{r0}, presented in Fig. 1. Impact trajectories are defined as those possessing a position vector that, at any time, passes on or within the radius of the body P_2. Escape trajectories are identified by an x-coordinate lying more than 0.01 nondimensional units beyond either L_1 or L_2.

3. Short-term behavior near P_2

An investigation of short-term orbits is based on the construction of periapsis Poincaré maps. For a given Jacobi value, a region on the surface of section is isolated within the zero-acceleration contour that forms the boundary between periapses and apoapses [18]. A set of initial periapse conditions is then defined within the contour. Each point within the region corresponds to the initial condition associated with a specific planar prograde trajectory about P_2; each trajectory is propagated forward in time for one revolution to its subsequent periapsis. Four possible outcomes of this propagation exist: the spacecraft impacts P_2; the spacecraft escapes out the L_1 gateway; the spacecraft escapes through the L_2 gateway; or, the spacecraft remains captured near P_2, that is, it continues to evolve within the ZVCs. Each point within the contour is colored consistent with the outcome of the propagation: black corresponds to impact, blue reflects escape out L_1, red indicates escape through L_2, and gray signifies an orbit that remains captured. As an example, consider a spacecraft in the vicinity of Saturn in the Sun–Saturn system. For a Jacobi value $J=J_1=3.0173046596239$ $(J<J_{L_2})$, each initial condition within the contour is propagated forward to its next periapsis; the integration is terminated early if the state reaches escape or impact. The resulting map appears in Fig. 3a. Note that well-defined lobes exist that identify the escape and impact trajectories. These lobes are analogous to the lobes defined for the HR3BP by Villac and Scheeres [11] and Paskowitz and Scheeres [12]. In the planar case, the lobes are outlined by the stable manifolds of the L_1 and L_2 Lyapunov orbits [19]. As is well known, planar trajectories that lie within the stable manifold tubes of the Lyapunov orbits escape from the vicinity of Saturn [7]. The lobes represent regions in which a periapsis occurs just prior to direct escape from the vicinity of

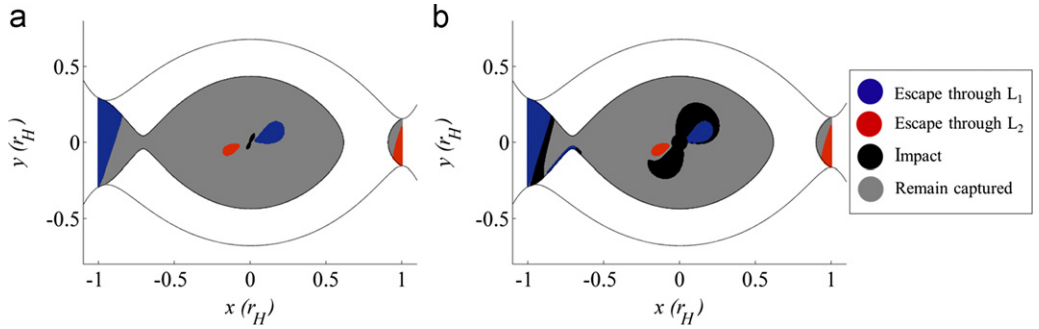

Fig. 3. Initial condition map for one revolution, Sun–Saturn system (a) and Saturn–Titan system (b). (For interpretation of the references to color in this figure legend, the reader is referred to the web version of this article.)

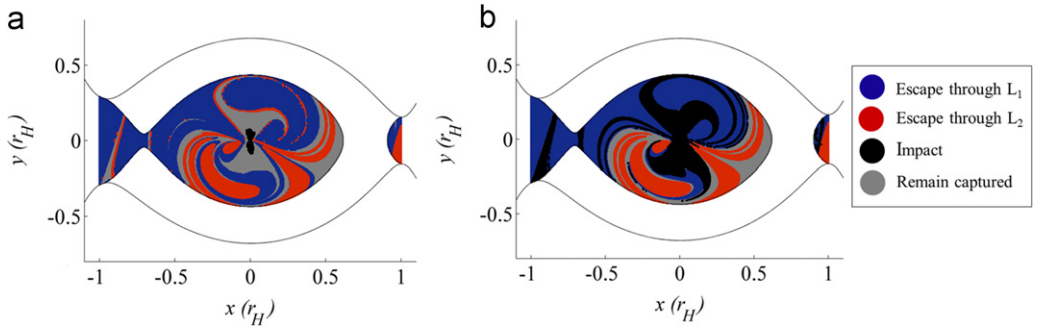

Fig. 4. Initial condition map for six revolutions, Sun–Saturn system (a) and Saturn–Titan system (b).

Saturn; any trajectory with a periapsis in one of these lobes escapes prior to reaching its next periapsis. These lobes can, therefore, be considered gateways to escape: all escaping trajectories pass through one of these regions at the final periapse passage prior to escape. Similarly, the black regions represent initial conditions associated with orbits that impact Saturn prior to the next periapse passage.

If the initial conditions are propagated for a longer span of time, a similar initial condition map is created. Fig. 4a represents an initial condition map that results when each trajectory is propagated for up to 6 revolutions. Again, integration is terminated if the trajectory escapes or impacts Saturn; if it reaches its 6th periapse passage without impacting or escaping, it is still classified as captured. As before, the colors represent the fate of each trajectory. As expected, during the longer propagations, more trajectories escape or impact Saturn. The lobes from Fig. 3 remain; they are joined by additional regions of escape and impact. A single trajectory's periapses cycle through the lobes in a predictable pattern.

The characteristics of the maps change when (i) the energy level is increased or decreased, or (ii) the mass parameter is altered—that is, when the maps are computed in a different system. An equivalent set of maps for the Saturn–Titan system appears in Figs. 3b and 4b. The Saturn–Titan system possesses a mass parameter that is similar in value to that of the Sun–Saturn system. Thus, for an equivalent energy level, the regions of escape are similar in appearance in the two systems. However, in units of Hill radii, Titan's radius is much larger than that of Saturn and, consequently, many more initial states lead to impact in the Saturn–Titan system as compared to the Sun–Saturn system. It is clear from Fig. 4b that few trajectories at this energy level remain in orbit about Titan after 6 revolutions. Analogous lobes are created for out-of-plane trajectories. Examples appear in Davis and Howell [19].

A closer investigation of trajectories that remain in orbit about the smaller primary after a single revolution yields information about the effects of tidal acceleration on the orbits. In Fig. 5, each initial state in the Sun–Saturn system that remains in orbit after a single revolution is colored according to the change in periapse radius from one periapsis to the next. Solar gravity results in a rise in the periapse distance in trajectories represented in red. Initial states colored blue experience a decrease in periapse radius over one revolution. It is apparent that trajectories oriented in quadrants I and III experience a decrease in periapse radius over one revolution, while trajectories in quadrants II and IV undergo an increase in periapse radius during a single orbit. This broad look at the design space is consistent with the analysis of solar gravity by quadrants summarized above.

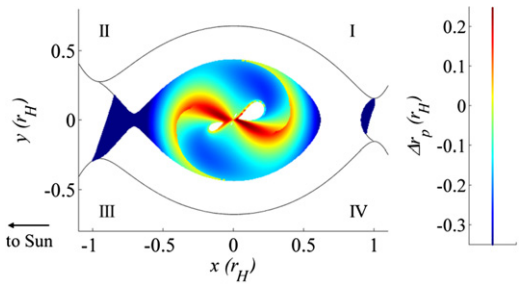

Fig. 5. Change in r_p over one revolution for captured trajectories in the Sun–Saturn system; $J=J_1$. (For interpretation of the references to color in this figure legend, the reader is referred to the web version of this article.)

4. Long-term behavior near P_2

The initial condition maps above relate initial periapses to the fate of the trajectory after a single revolution, revealing information about the short-term behavior of the full set of trajectories. Another type of periapsis Poincaré map is useful for the investigation of the long-term evolution of trajectories in the vicinity of P_2 in the CR3BP. Long-term periapsis Poincaré maps are created with a surface of section at periapsis; the state of each periapsis as the trajectory evolves is recorded over a long-term propagation. Particular attention is focused on the gray regions of the initial condition maps appearing in Fig. 4, that is, trajectories that remain captured about the smaller primary over long-term intervals.

Each long-term trajectory is characterized by the pattern that is formed by its periapses as the trajectory evolves over time. In the Sun–Saturn system, at an energy level such that $J=J_1$, four types of periapse profiles are evident for long-term trajectories. Such trajectories are classified as figure 8-type, hourglass-type, lobe-type, or arrowhead-type trajectories. See Davis and Howell [19] for further discussion. An example of each type of trajectory appears in Fig. 6, with periapses plotted in black over each colored trajectory.

Consider a large set of trajectories in the planar Sun–Saturn system characterized by a Jacobi value $J=J_1$ such that the ZVCs are open at both L_1 and L_2. Approximately 11,000 initial periapse states are defined in the vicinity of Saturn. Each initial state is propagated for approximately 33 revolutions of the primaries: equivalent to 1000 years in the Sun–Saturn system. Some of the trajectories escape from the vicinity of Saturn during the course of the propagation; others remain captured over the full time span. As each trajectory evolves, the spacecraft state is recorded at each periapse passage. The coordinates y_p versus x_p, relative to the rotating frame, are plotted on a map as the trajectories evolve over ~33 periods of the primaries. For $J=J_1$, the map appears in Fig. 7. The Saturn-centered view focuses on the trajectories that remain captured for the duration of the propagation. The map consists of two main regions. First, an hourglass-shaped region is comprised of points corresponding to captured trajectories. Trajectories associated with three of the periapse profile types combine to create this region—figure 8-type trajectories, lobe-type trajectories, and hourglass-type trajectories. A second region exists to the left of the hourglass, centered about $y_p=0$; it is composed of periapse points belonging to arrowhead-type trajectories. Surrounding these two regions is a large zone corresponding to trajectories that eventually escape.

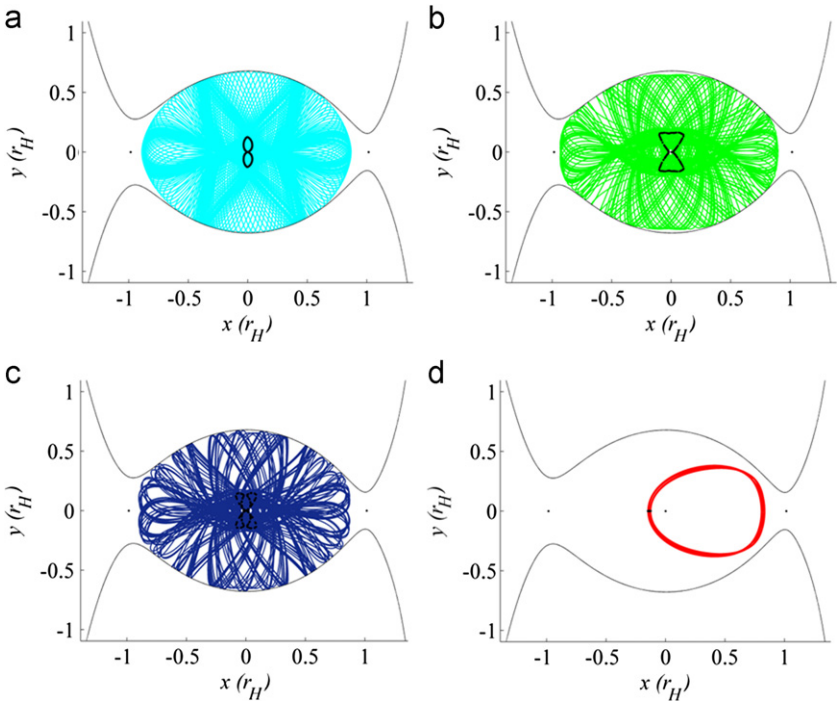

Fig. 6. Sample trajectories corresponding to each periapse profile for $J=J_1$ in the Sun–Saturn system, with periapses plotted in black. Fig. 8 (a), hourglass (b), lobe (c), and arrowhead (d) trajectories.

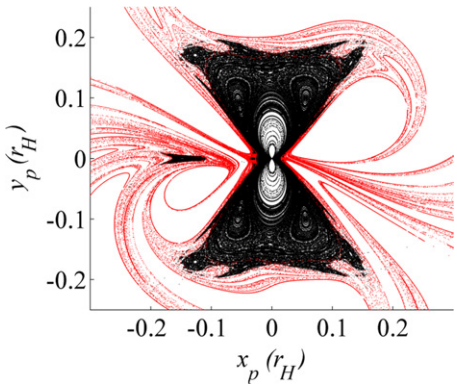

Fig. 7. Periapsis Poincaré map displaying y_p vs. x_p for 1000 years for trajectories in the Sun–Saturn system with $J=J_1$, $0.07r_H < r_{p0} < 0.25r_H$, $0 < \omega_{r0} < \pi$. (For interpretation of the references to color in this figure legend, the reader is referred to the web version of this article.)

The stable manifold trajectories associated with the L_1 and L_2 Lyapunov orbits at this value of Jacobi constant are represented by the red points in Fig. 7. Note how the regions of captured trajectories are neatly outlined by the stable manifold tubes. Islands associated with periodic trajectories exist within the periapsis Poincaré map. The center point in each of these sets of islands corresponds to a periodic trajectory.

Recall that by employing the short-term initial condition maps discussed above, the location of an initial periapsis reveals the fate of the trajectory over one revolution. In the same way, the location of periapsis in x–y space defines the periapse profile and therefore the behavior of a planar trajectory over a long-term propagation. A schematic appears in Fig. 8. Each colored zone represents a periapse profile type. If a trajectory possesses a periapsis located in one of the colored zones, every periapsis over a long-term propagation will also lie within the same colored zone. For example, if a trajectory with $J=J_1$ in the Sun–Saturn system possesses an initial periapsis state within the light blue region, the trajectory is characterized as a figure 8-type trajectory, and each periapsis over a long-term propagation will remain within the light blue region. Similarly, any trajectory originating from a periapsis within the black region will eventually impact Saturn. A periapsis lying within the dark blue region corresponds to a lobe-type trajectory, and within the green region to an hourglass-type trajectory. Periapses located in the purple regions also belong to hourglass-type trajectories; however, the periapses along these paths remain within discrete regions, yielding quasi-periodic trajectories. The red zone is comprised of periapses from arrowhead-type trajectories, and any trajectory with an initial periapsis within the white region will escape from the vicinity of Saturn over a long-term propagation. The schematic in Fig. 8 is specific to the mass parameter and Jacobi constant associated with one set of trajectories; changing either of these parameters will change the characteristics of the schematic. This schematic may be used in a design process; simply by placing an initial periapsis within one of the colored regions at the specified value of Jacobi integral, a designer is certain to achieve a trajectory with particular characteristics. Note, however, that the boundaries between the regions are imprecise. Close to the edges of the regions, trajectories

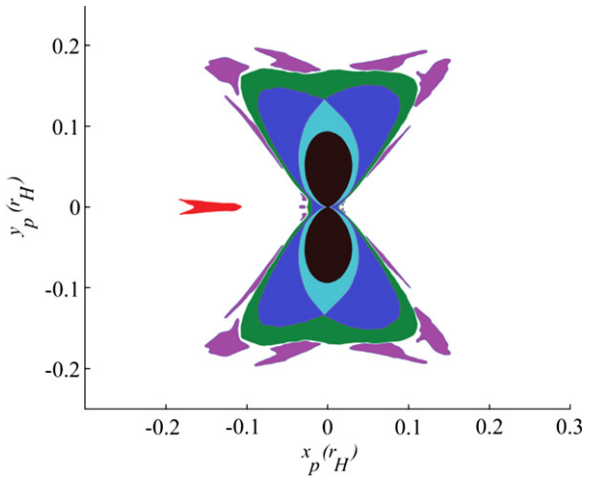

Fig. 8. Periapse profile schematic. Black corresponds to impact trajectories, light blue to figure 8-type trajectories, dark blue to lobe-type trajectories, green to hourglass-type trajectories, purple to quasi-periodic hourglass-type trajectories, red to arrowhead-type trajectories, and white to escaping trajectories. (For interpretation of the references to color in this figure legend, the reader is referred to the web version of this article.)

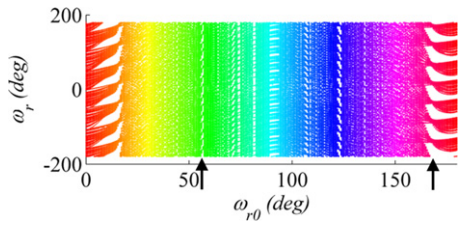

Fig. 9. Periapse angles over time, ω_r, plotted against initial periapse angles ω_{r0}. Sun–Saturn system, $J=J_1$, $r_{p0}=0.12r_H$, and $\phi=68.8^\circ$. Quasi-periodic orbits result in discrete values of ω_r over time; two such orbits are marked with arrows.

may exhibit characteristics of both types of trajectories, or they may flip from one type of trajectory to another. The schematic provides a quick, methodical way to identify trajectories with certain types of behaviors.

The selection of different variables for display in a periapsis Poincaré map highlights various trajectory characteristics that are easily identifiable. Consider a set of initial conditions in the Sun–Saturn system corresponding to initial radius $r_{p0}=0.12r_H$ and $J=J_1$. If the initial periapse radius is fixed, then each initial condition corresponds to a specific initial periapse angle, ω_{r0}, as defined in Fig. 1. As the path evolves, subsequent periapses occur at varying periapse distances, r_p, and periapse orientation angles, ω_r. Since r_{p0} is constant, a single trajectory is identified by its initial angle, ω_{r0}; then, the evolving periapse angles, ω_r, are plotted over time for a given ω_{r0}. All trajectories are reflected in one map if all subsequent periapse angles ω_r are plotted for each initial periapse angle, ω_{r0}. This type of map is useful for locating quasi-periodic trajectories, which possess periapse angles ω_r over time only for discrete, repeating values. Such trajectories, both in the planar and 3D cases, are easily located by inspection from such a map. An example of a map of ω_r vs. ω_{r0} appears in Fig. 9 for an initial velocity angle $\phi=68.8^\circ$. Each vertical line represents a single trajectory; each point is colored according to its initial periapse angle ω_{r0}. Two examples of quasi-periodic trajectories are marked with arrows on the map, though other quasi-periodic orbits are also apparent. Note that the discrete, repeating values of ω_r exist as the trajectory evolves for each quasi-periodic orbit. The corresponding values of ω_{r0} produce quasi-periodic orbits in the rotating frame; the two 3D quasi-periodic trajectories clearly identified from the ω_r vs. ω_{r0} map appear in Fig. 10a and b. Each path is propagated for ~33 periods of the primaries, or 1000 years. Orbits of both low-order and high-order resonance are located by inspection from the map. In both the planar and 3D cases, quasi-periodic trajectories are computed without requiring a correction

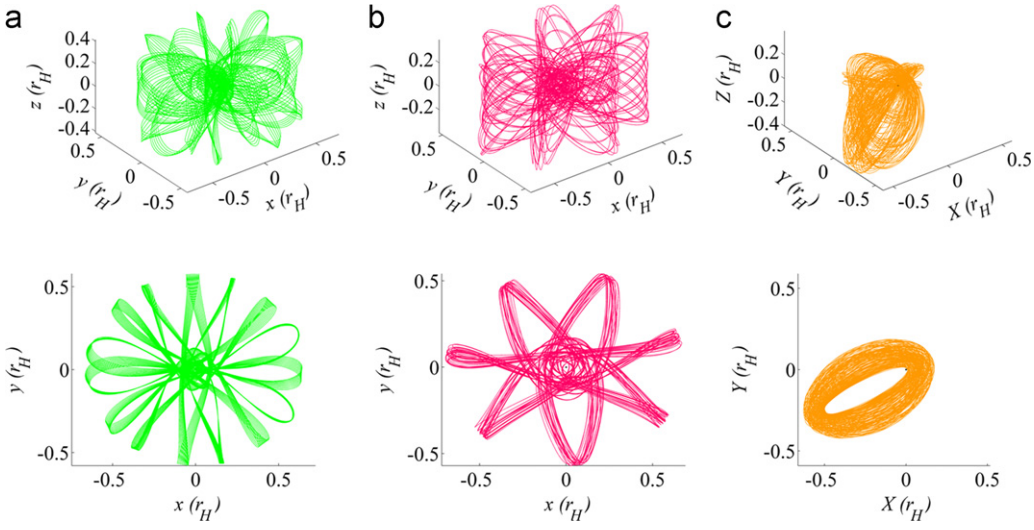

Fig. 10. Two 3D quasi-periodic orbits viewed in the rotating frame (a, b), and a 3D trajectory with a near-stationary line of apsides viewed in the inertial frame (*c*), with *x*–*y* projections (bottom) for $r_{p0}=0.12r_H$, $z_0=0$, and $\phi=68.8^\circ$.

or targeting algorithm—the initial conditions selected directly from the map are simply propagated.

A similar map is used to locate trajectories that have slowly-varying lines of apsides in the inertial frame. A map correlating the argument of periapsis in the inertial frame, denoted ω_i, to an initial periapse angle in the rotating frame, ω_{r0}, is employed to locate orbits with near-stationary or slowly varying values of ω_i, as well as trajectories that are quasi-periodic in the inertial frame. Quasi-periodic trajectories possess arguments of periapsis in fixed ranges, rather than continuously over the range $0–2\pi$. An example of an orbit with a nearly-stationary line of apsides and a velocity angle $\phi=68.8^\circ$ appears in Fig. 10c in an inertial view. In summary, trajectories that would otherwise be quite difficult to locate are easily selected off various periapsis Poincaré maps.

5. Examples: trajectory design for Cassini end-of-mission options

After an impressive tour of Saturn, and as the Cassini mission was originally winding down, safe disposal of the spacecraft was a priority. However, developing trajectory options for an end-of-life scenario for a spacecraft already established in its orbit with a limited amount of propellant remaining is always challenging. Working within this framework, in 2007 a preliminary Cassini end-of-life design study was completed [17,20–22]. As a part of the original investigation, one potential scenario for the final phase of the Cassini mission was to leverage solar perturbations with Titan encounters and small maneuvers to enable the spacecraft to reach various end-of-mission destination orbits. After employing a trial-and-error approach to complete the analysis and deliver several point-solution trajectories, it was clear that a more methodical technique would be valuable for future applications. With this motivation, a new effort was undertaken to explore the design space more thoroughly; periapsis Poincaré maps were employed to organize the design space and to allow a more direct selection of trajectories that can satisfy various mission objectives. Given this alternate parameterization, some of the Cassini options are re-visited to demonstrate an alternative design process.

5.1. Example 1

As a first example, consider the Cassini end-of-life problem. Spacecraft disposal options included escape from Saturn and impact into the planet. Titan flybys can deliver the Cassini spacecraft to a desired orbit, which is characterized by a particular value of Sun–Saturn Jacobi constant. The initial condition map corresponding to the Jacobi constant of one post-flyby trajectory option, $J=3.106$, appears in Fig. 11. At this energy level, it is apparent that, depending on the location of periapsis, the trajectory can either impact Saturn, escape through the L_1 or L_2 gateways, or remain in orbit about Saturn. In the Sun–Saturn frame, given r_p, the periapsis of the orbit can lie anywhere on a Saturn-centered ring, its periapse angle depending on the relative orientation of the three bodies

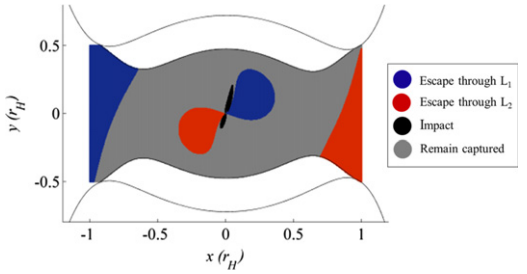

Fig. 11. Initial condition map for a post-flyby Cassini end-of-life trajectory.

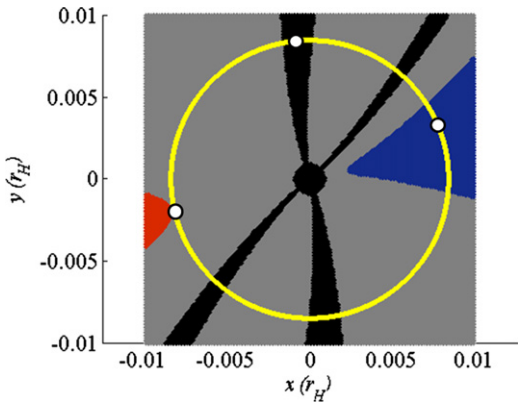

Fig. 12. Initial condition map for a post-flyby Cassini end-of-life trajectory: zoomed view. (For interpretation of the references to color in this figure legend, the reader is referred to the web version of this article.)

at the time of the flyby. For the scenario described above, this ring appears in yellow in Fig. 12, overlaid on a zoomed view of the initial conditions map. From this figure, the appropriate orientation of periapsis is immediately apparent to achieve either escape through L_1 or L_2 (place periapsis in the blue and red regions, respectively) or impact into Saturn (place periapsis in a black region). Three sample orbits, originating from the three white markers in Fig. 12, are plotted in Fig. 13. Clearly, the selection of the initial periapse angle results in the desired outcome in each case. This approach is an improvement over the technique used in the tidal acceleration investigation in the original Cassini end-of-life analysis [17]; instead of using a trial-and-error procedure to determine the correct energy level and orientation required to achieve an impact or escape trajectory, the desired orbit is methodically selected from the map.

5.2. Example 2

In a second application, a design strategy combines an initial condition map with a long-term periapsis Poincaré map to achieve a potential Cassini end-of-life orbit beyond the irregular, retrograde orbit of Phoebe. Phoebe's semi-major axis is 214 R_S (1 R_S=60,268 km), which corresponds to a period of 1.5 years. Within the constraints of the Cassini end-of-life scenario, a transfer from some likely spacecraft trajectory at end-of-mission into a

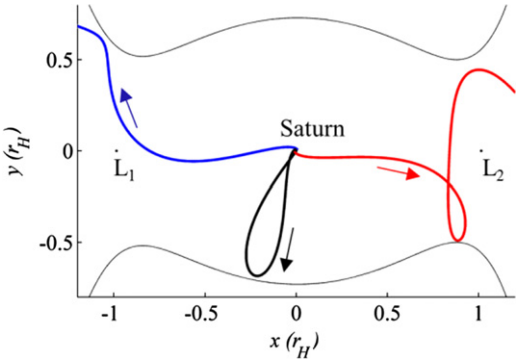

Fig. 13. Sample impact and escape trajectories originating from periapses marked in Fig. 19.

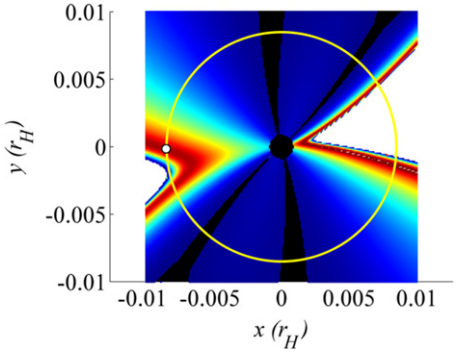

Fig. 14. Initial condition map colored according to Δr_p over one revolution. The selected initial condition lies in a deep red zone, corresponding to an increase in periapse radius. (For interpretation of the references to color in this figure legend, the reader is referred to the web version of this article.)

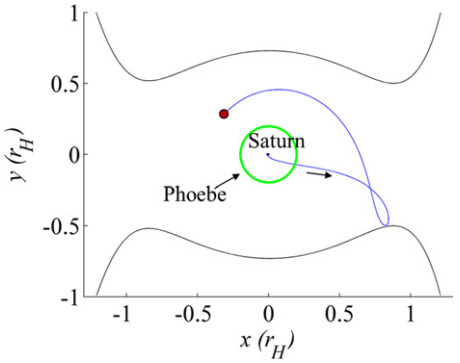

Fig. 15. Trajectory corresponding to the selected initial condition. Maneuver location at the second periapsis is marked in red. (For interpretation of the references to color in this figure legend, the reader is referred to the web version of this article.)

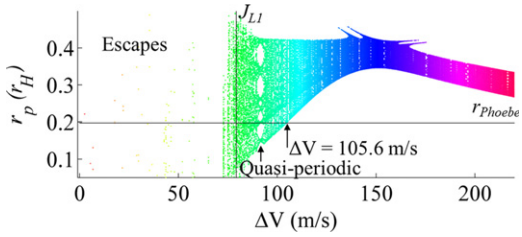

Fig. 16. Periapsis Poincaré map for the long-term Cassini end-of-life option. The selected trajectory is marked with an arrow.

very long-term, Saturn-centered trajectory that remains continuously beyond the orbit of Phoebe cannot be accomplished solely with Titan encounters and a maneuver or ΔV, since the required maneuvers are prohibitively large. Instead, solar perturbations are leveraged to reduce the magnitude of the required ΔV. Thus, the goal in this example is twofold: (i) to employ the Sun's gravity to raise periapsis significantly, at which point, (ii) a maneuver is applied to circularize the trajectory such that the excursions of the periapsis distance over time are reduced, even under the very sizable effects from multiple gravitational forces. The focus is therefore on post-flyby trajectories that remain captured in the system after one revolution, that is, the gray regions in Fig. 12. Since the first goal is to raise the second periapse radius, the map from Fig. 12 is re-plotted in Fig. 14; the colors now reflect new information. Each initial periapsis (represented by a point on the map) is now colored consistent with the change in periapse radius after one revolution. This colored map appears in Fig. 14 for the same Jacobi constant, $J=3.016$. The blue regions indicate a decrease in r_p (note that the impact zones exist in the midst of the deepest blue, indicating the largest decrease in r_p) and the red regions correspond to the greatest increase in periapse distance. By orienting the post-flyby periapsis in a region of sufficiently increased r_p, periapsis is raised above Phoebe's orbit. The selected post-flyby trajectory appears in Fig. 15.

It is now necessary to address the second step and implement a maneuver at the second periapsis (marked in red in Fig. 15) to achieve a long-term orbit that neither impacts nor escapes for at least 500 years, as specified by the Cassini end-of-life requirements. The maneuver is assumed to be tangent to the spacecraft velocity. To facilitate the selection of the ΔV magnitude, a long-term periapsis Poincaré map is produced to examine the possible post-maneuver trajectories. A set of potential trajectories is created by varying the magnitude of the maneuver from 0 to 250 m/s. Each trajectory is propagated for 500 years, and the periapse radii over time are recorded and plotted against ΔV magnitude in a map appearing in Fig. 16. Marked on the map are lines that highlight the ΔV required to close the L_1 gateway as well as the orbital radius of Phoebe. From this map, it is straightforward to select the minimum value of ΔV that is required such that a trajectory will not escape or that the periapsis will remain above the orbit of Phoebe for the 500-year propagation time. Also apparent are quasi-periodic trajectories; a similar map of ω_i versus ΔV allows selection of trajectories that display quasi-periodic behavior in the inertial frame. One particular solution requires a $\Delta V=105.6$ m/s. This orbit remains beyond the orbit of Phoebe and displays quasi-periodic behavior in both the rotating and inertial frames. It appears in Fig. 17. A combination of initial condition maps and long-term periapsis Poincaré maps allows easy selection of orbits for preliminary trajectory

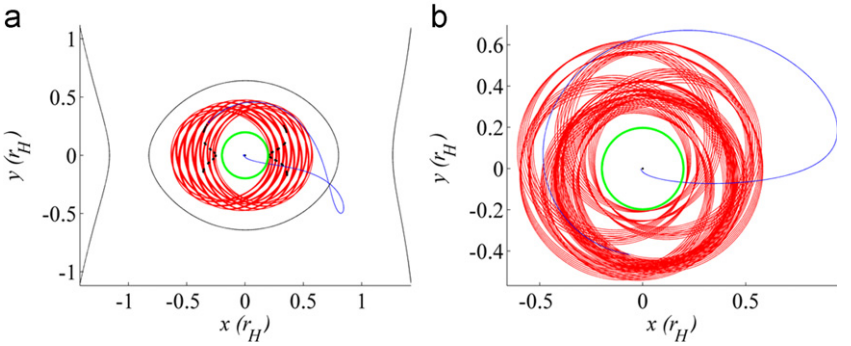

Fig. 17. Post-flyby Cassini trajectory for long-term end-of-life option in rotating (a) and inertial (b) views. Phoebe's orbital radius is marked in green, the post-flyby trajectory is blue, and the post-ΔV trajectory is red. (For interpretation of the references to color in this figure legend, the reader is referred to the web version of this article.)

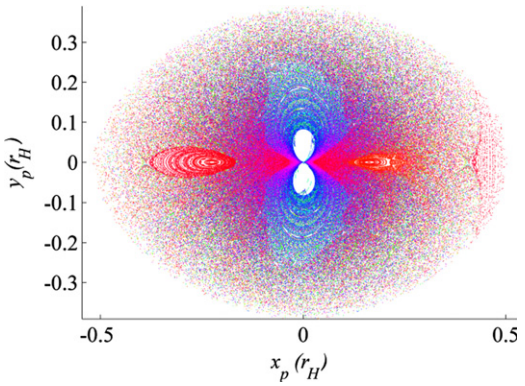

Fig. 18. Periapsis Poincaré map for 2844 trajectories in the Saturn–Titan system, each propagated for 1.44 years.

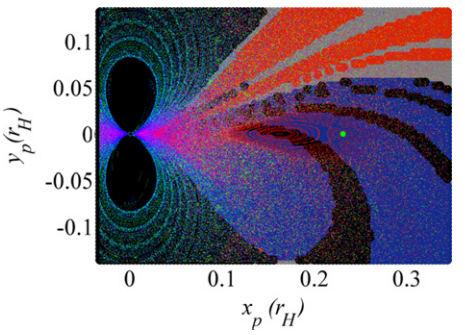

Fig. 19. Long-term map at $J=J_{L_1}$ overlaid on initial condition map at $J=J_2$; periodic trajectory marked in green lies in the lobe corresponding to the second periapsis after entrance into the vicinity of Titan through L_1. (For interpretation of the references to color in this figure legend, the reader is referred to the web version of this article.)

design in the tidally-influenced environment. These maps also lend insight into the characteristics of the design space.

6. Example: trajectory design for Titan capture

Potential applications are not limited to the Sun–Saturn system. In this example, periapsis Poincaré maps are used to design a capture into a periodic orbit about Titan. Consider a spacecraft in the Saturn–Titan system with an energy level such that ZVCs are open at L_1 and L_2 ($J_2 = 3.015311017945150 < J_{L_2}$). Recall that the initial condition map in Fig. 4b represents regions of escape from Titan's vicinity after up to 6 revolutions of the spacecraft. If this map is reflected across the x-axis, time is reversed; that is, the reflected map corresponds to regions of entrance into the region near Titan through the gateways at L_1 and L_2. In this map, the blue regions correspond to periapses of trajectories entering through L_1 into orbit at Titan, while the red lobes are comprised of periapses of orbits entering the vicinity of Titan through L_2.

By applying ΔV at a selected periapsis of one of these entering trajectories, the energy level of that trajectory is reduced with the goal to reach a quasi-periodic orbit about Titan. To achieve this objective, however, the particular trajectory must be carefully selected. To ensure that the orbit remains centered at Titan, the energy level

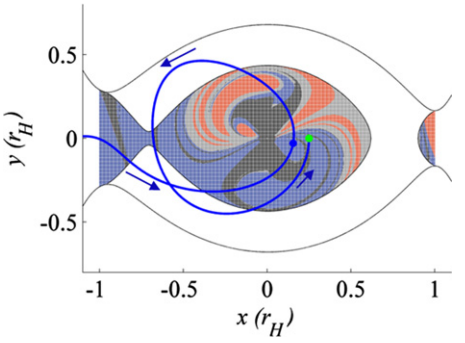

Fig. 20. Initial condition map in the Saturn–Titan system; blue regions represent trajectories entering through the L_1 gateway while red regions correspond to trajectories approaching Titan through the L_2 gateway. Overlaid on the map is a sample capture trajectory; its first periapsis after capture is marked in blue, its second in green. (For interpretation of the references to color in this figure legend, the reader is referred to the web version of this article.)

is chosen to just close off the L_1 gateway, that is, $J=J_{L_1}$. A long-term periapsis Poincaré map is created by propagating 2844 trajectories for 33 periods of the primaries. In the Saturn–Titan system, this corresponds to approximately 1.44 years. Initial conditions are chosen such that $0.049 \quad r_H < r_{p0} < 0.4 \quad r_H$ and $0 < \omega_0 < \pi$. The map of

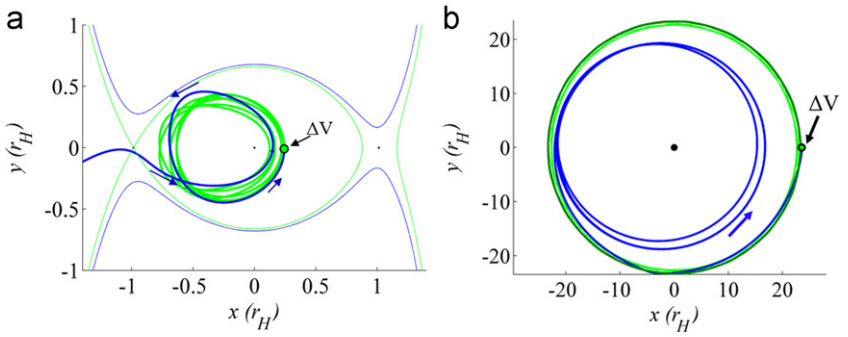

Fig. 21. Titan capture trajectory in the Titan-centered rotating view (a) and the Saturn-centered inertial view (b). Spacecraft enters the vicinity of Titan on the blue trajectory; at the second periapsis (marked in green), a ΔV is applied to achieve the green periodic trajectory. (For interpretation of the references to color in this figure legend, the reader is referred to the web version of this article.)

y_p versus x_p over time appears in Fig. 18. The periapses of each trajectory are colored according to the orbit's initial periapse angle, ω_0. From this map, it is clear that regions of quasi-periodic trajectories exist centered at $\omega_0=0$ and $\omega_0=\pi$. Three periodic trajectories are located at the center of these islands. They correspond to approximately $r_{p0}=0.163\ r_H$ and $r_{p0}=0.231\ r_H$ at $\omega_0=0$, and $r_{p0}=0.225\ r_H$ at $\omega_0=\pi$.

By overlaying the long-term map in Fig. 18 on the initial condition map, it is simple to determine which long-term orbits with $J=J_{L_1}$ can be achieved by applying ΔV at periapsis soon after entering the vicinity of Titan at an energy level corresponding to $J=J_2$. A zoomed view of the overlaid maps appears in Fig. 19. Consider the periodic orbit with $J=J_{L_1}$ and with periapsis located at $r_{p0}=0.231\ r_H$ and $\omega_0=0$. This coordinate is marked in green in Fig. 19. The corresponding trajectory is located in the lobe associated with the second periapsis after L_1 capture. That is, the trajectory enters through the L_1 gateway and reaches the desired location at its second periapsis passage in the vicinity of Titan (see Fig. 20). When the trajectory passes through this periapsis, a ΔV of 7.4 m/s is applied to lower the energy so that $J=J_{L_1}$. The resulting quasi-periodic trajectory appears in the Titan-centered rotating frame in Fig. 21a and in a Saturn-centered inertial view in Fig. 21b. It is propagated for 1.44 years, equivalent to 33 periods of the primaries. By combining initial condition maps corresponding to entrance into the vicinity of Titan with long-term periapsis Poincaré maps, a capture into a quasi-periodic orbit about Titan is methodically designed.

7. Summary and concluding remarks

In this investigation, periapsis Poincaré maps are employed to reveal characteristics in groups of trajectories over both short-term and long-term propagations. Both planar and 3D trajectories are considered, with a focus on the Sun–Saturn and Saturn–Titan systems. To categorize velocity in the 3D case, a velocity angle is introduced in the plane perpendicular to the radius vector. Initial condition maps are generated to highlight the behavior of trajectories over short-term. In both the planar and 3D cases, lobes are defined that can be considered gateways to escape (and by symmetry, capture) through L_1 and L_2. Long-term trajectory evolution is also examined. For a given value of Jacobi constant in the Sun–Saturn system, periapsis Poincaré maps are generated for large sets of trajectories over extended propagations. These maps allow prediction of long-term trajectory behavior based on the location and energy level of the initial periapsis. They also provide a simple method of locating periodic, quasi-periodic, and quasi-frozen orbits about the smaller primary.

Without analytical relationships in CR3BP, numerical tools are a necessary component of any design algorithm in this regime. With better insight into the design space, it is possible to focus a search on the regions that are most useful for a particular application. If it is possible to recognize certain characteristic features that reappear in maps for different systems and energy levels, a designer can organize the information and use it to advantage when new designs are required.

The understanding of the design space offered by the short- and long-term maps is combined in several sample trajectory design applications, including a Cassini end-of-life example as well as a sample trajectory resulting in capture into orbit about Titan. Periapsis Poincaré maps provide a quick and efficient method for the selection of a trajectory to satisfy given mission requirements.

Acknowledgments

The authors thank the editor and the reviewers for their contributions in improving this paper. The authors also appreciate the assistance of Amanda Haapala with some of the computations. This research was supported in part through Zonta International's Amelia Earhart Fellowship and a Purdue Forever Fellowship. The authors also appreciate the support from the Purdue University College of Engineering and the School of Aeronautics and Astronautics.

References

[1] E.A. Belbruno, Lunar capture orbits, a method of constructing Earth Moon trajectories and the Lunar GAS Mission, in: Proceedings of

the AIAA/DGLR/JSASS International Electric Propulsion Conference, AIAA Paper No. 1987-1054, Colorado Springs, Colorado, May 1987.
[2] E.A. Belbruno, J.K. Miller, Sun-perturbed Earth-to-Moon transfers with ballistic capture, Journal of Guidance, Control, and Dynamics 16 (4) (1993) 770–775.
[3] H. Yamakawa, J. Kawaguchi, N. Ishii, H. Matsuo, On Earth–Moon transfer trajectory with gravitational capture, in: Proceedings of the AAS/AIAA Astrodynamics Specialist Conference, AAS Paper No. 93-633, Victoria, Canada, August 1993.
[4] J. Kawaguchi, H. Yamakawa, T. Uesugi, H. Matsuo, On making use of lunar and solar gravity assists in LUNAR-A, PLANET-B missions, Acta Astronautica 35 (9–11) (1995) 633–642.
[5] K.C. Howell, M. Kakoi, Transfers between the Earth–Moon and Sun–Earth systems using manifolds and transit orbits, Acta Astronautica 59 (2006) 367–380.
[6] W.S. Koon, M.W. Lo, J.E. Marsden, S.D. Ross, Shoot the Moon, in: Proceedings of the AAS/AIAA Astrodynamics Specialist Conference, AAS Paper No. 2000-166, Clearwater, Florida, August 2000.
[7] G. Gómez, W.S. Koon, M.W. Lo, J.E. Marsden, J. Masdemont, S.D. Ross, Invariant manifolds, the spatial three-body problem, and space mission design, in: Proceedings of the AAS/AIAA Astrodynamics Specialist Conference, AAS Paper No. 2001-301, Quebec City, Canada, August 2001.
[8] J.S. Parker, G.H. Born, Modeling a low-energy ballistic lunar transfer using dynamical systems theory, Journal of Spacecraft and Rockets 45 (6) (2008) 1269–1281.
[9] R.P. Russell, T. Lam, Designing capture trajectories to unstable periodic orbits around Europa, in: Proceedings of the AAS/AIAA Spaceflight Mechanics Meeting, AAS Paper No. 2006-189, Tampa, Florida, January 2006.
[10] K.C. Howell, B.G. Marchand, M.W. Lo, Temporary satellite capture of short-period Jupiter family comets from the perspective of dynamical systems, in: Proceedings of the AAS/AIAA Spaceflight Mechanics Meeting, Clearwater, Florida, January 2000.
[11] B.F. Villac, D.J. Scheeres, Escaping trajectories in the Hill three-body problem and applications, Journal of Guidance, Control, and Dynamics 26 (2) (2003) 224–232.
[12] M.E. Paskowitz, D.J. Scheeres, Robust capture and transfer trajectories for planetary satellite orbiters, Journal of Guidance, Control, and Dynamics 29 (2) (2006) 342–353.
[13] B.F. Villac, D.J. Scheeres, New class of optimal plane change maneuvers, Journal of Guidance, Control and Dynamics 26 (5) (2003) 750–757.
[14] V. Szebehely, Theory of Orbits: The Restricted Problem of Three Bodies, Academic Press, New York, 1967.
[15] D.P. Hamilton, J.A. Burns, Orbital stability zones about asteroids, Icarus 92 (1991) 118–131.
[16] B.F. Villac, D.J. Scheeres, L.A. D'Amario, M.D. Guman, The effect of tidal forces on orbit transfers, in: Proceedings of the AIAA/AAS Spaceflight Mechanics Meeting, AAS Paper No. 01-247, Santa Barbara, California, February 2001.
[17] D.C. Davis, C. Patterson, K.C. Howell, Solar gravity perturbations to facilitate long-term orbits: application to Cassini, in: Proceedings of the AAS/AIAA Astrodynamics Specialist Conference, AAS Paper No. 07-275, Mackinac Island, Michigan, 19–23 August, 2007.
[18] D.C. Davis, K.C. Howell, Trajectory evolution in the multi-body problem with applications in the Saturnian System, in: Proceedings of the 61st IAF International Astronautical Congress, Paper No. IAC-10-C1.1.7, Prague, Czech Rebublic, September 2010.
[19] D.C. Davis, K.C. Howell, Long-term evolution of trajectories near the smaller primary in the restricted problem, in: Proceedings of the AAS/AIAA Space Flight Mechanics Meeting, AAS Paper No. 10-184, San Diego, California, February 2010.
[20] C.H. Yam, D.C. Davis, J.M. Longuski, K.C. Howell, Saturn impact trajectories for Cassini end-of-mission, Journal of Spacecraft and Rockets 46 (2) (2009) 353–364.
[21] C. Patterson, M. Kakoi, K.C. Howell, C.H. Yam, J.M. Longuski, 500-Year eccentric orbits for the Cassini spacecraft within the Saturn system, in: Proceedings of the AAS/AIAA Astrodynamics Specialist Conference, AAS Paper No. 07-256, Mackinac Island, Michigan, 19–23 August, 2007.
[22] M. Okutsu, C.H. Yam, J.M. Longuski, N.J. Strange, Cassini end-of-life escape trajectories to the outer planets, in: Proceedings of the AAS/AIAA Astrodynamics Specialist Conference, AAS Paper No. 07-258, Mackinac Island, Michigan, 19–23 August, 2007.